ADVANCED MATERIALS TECHNOLOGIES
www.advmattechnol.de

A Dynamic Double-Flow Gut-On-Chip Model for Predictive Absorption Studies In Vitro

*Maria Elisabetta Federica Palamà, Maurizio Aiello, Gergő Borka, Jacopo Furci, Ilaria Parodi, Giuseppe Firpo, and Silvia Scaglione**

Human gut is crucial for digestion, drug absorption, and overall health; however traditional in vitro and animal models struggle to accurately replicate its complex mechanisms. This study introduces an innovative gut-on-chip based on the MIVO millifluidic device, designed to faithfully replicate the human intestinal environment. CaCo-2 and HT-29 cells were co-cultured under different ratio under dynamic flow conditions, resembling the bloodstream. Intestinal tissue differentiation was assessed through Trans-epithelial electrical resistance (TEER) measurements, Zonula Occludens-1, and Alcian blue staining. After model establishment, a second dynamic flow was applied on the apical side recapitulating the intestinal lumen niche. The dynamic culture conditions significantly reduced cell maturation time, obtaining a differentiated intestinal layer within 7-10 days, compared to 21 days of static culture. In addition, CaCo-2:HT-29 co-cultures enables to finely tune the mucus thicknesses and barrier function, essential for studying specific conditions. Furthermore, the introduction of a double apical-basal flow system recapitulated intestinal permeability characteristics more closely resembling those observed in vivo. The Double-Flow millifluidic Gut-on-Chip described and successfully validated enables to cross-correlate the barrier function of the epithelial layer with the CaCo-2:HT-29 cells ratios, finally providing a predictive model useful for drug development and disease modelling.

1. Introduction

Modelling the human intestine in the lab has become a significant challenge in recent years, due to its crucial roles in digestion,[1–3] absorption,[4,5] disease regulation[6–8] and immune function.[9–11] Most of the nutrients, food supplements and orally administered drugs are indeed absorbed through the intestinal tract, which thus serves as the primary body defence barrier against the external environment.[12] Moreover, beside the well-established pharmacokinetic and drug absorption studies,[13] as research on the human gut microbiome advances, in recent years intestine has been identified as a target for many human disease modelling and for efficacy studies on pre-/pro-/post-biotics.[14,15] Intestinal microbes have indeed been linked to numerous conditions, including indigestion, obesity, and immune-related diseases,[16,17] but also to neuro-cognitive[18] and skin disorders.[19,20]

In this scenario, the accurate in vitro modelling of the human gut represents a necessary milestone in drug development and disease treatment.[21] Among the currently available in vitro models, the human adenocarcinoma CaCo-2 cell line has been extensively used to test drug absorption and permeability, and for biopharmaceutics classification, being still recognized as a gold standard from a regulatory perspective.[22] However, this approach faces several limitations due to its

M. E. F. Palamà, M. Aiello, G. Borka, J. Furci, S. Scaglione
React4life S.p.A.
Genoa 16152, Italy
E-mail: s.scaglione@react4life.com
M. Aiello, I. Parodi, S. Scaglione
National Research Council of Italy
Institute of Electronic
Computer and Telecommunications Engineering (IEIIT)
Genoa 16149, Italy
The ORCID identification number(s) for the author(s) of this article can be found under https://doi.org/10.1002/admt.202401661

DOI: 10.1002/admt.202401661

G. Borka
University of Milan – Bicocca
Milan 20126
I. Parodi
Department of Computer Science
Bioengineering
Robotics and Systems Engineering
University of Genoa
Genoa 16126, Italy
G. Firpo
Department of Physics (DIFI)
University of Genoa
Genoa 16126, Italy

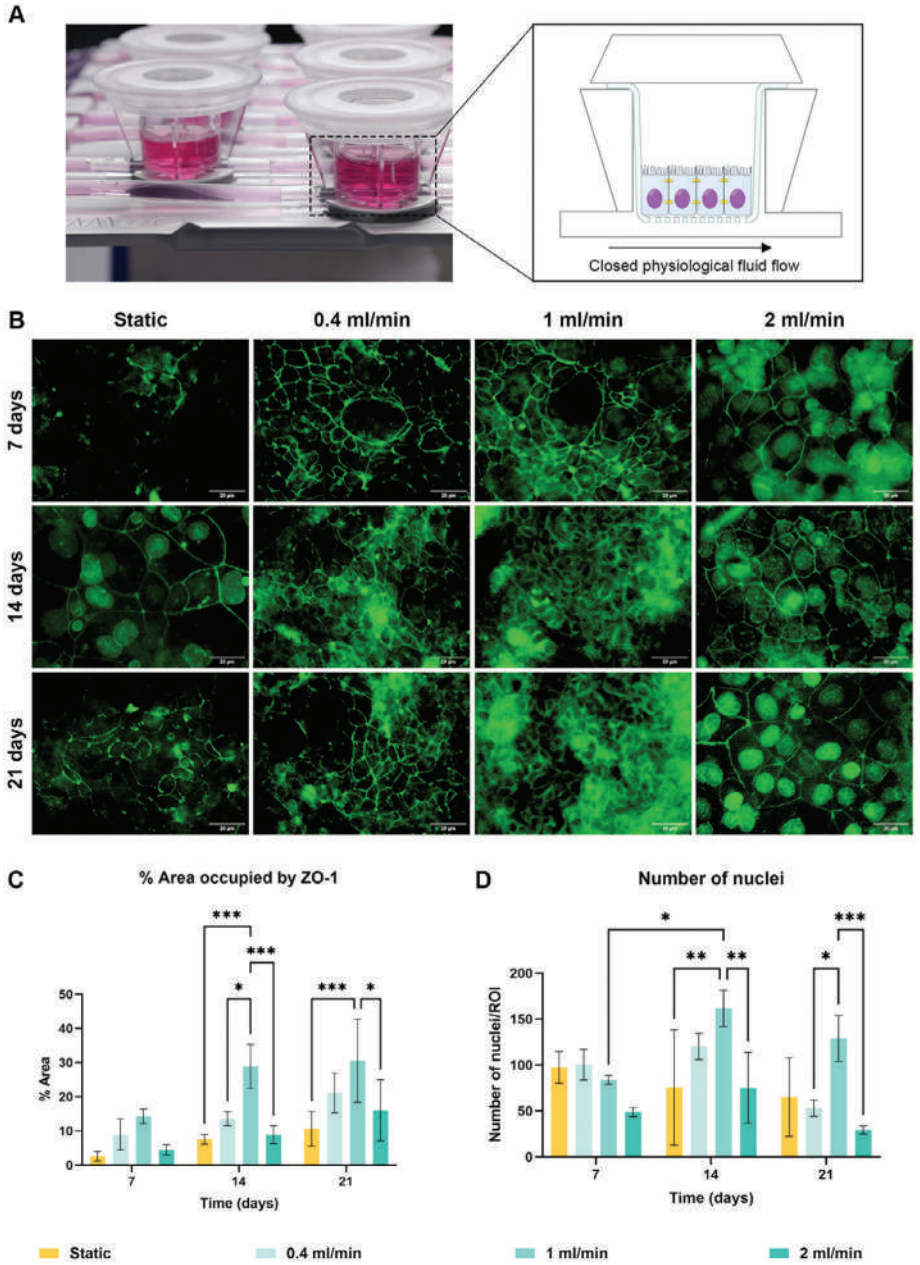

Figure 1. Analysis of CaCo-2 maturation levels in static and dynamic conditions through ZO-1 immunostaining. A) MIVO Single Flow chambers hosting the intestinal cell layers. The zoom reports a schematic representation of CaCo-2 cell line in MIVO Single Flow, cross-section. A closed physiological fluid flow resembling the capillary blood flow circulation is applied in the basal compartment, through a peristaltic pump. B) Representative figures of ZO-1 immunostaining at 7, 14, and 21 days in static or dynamic culture. Scale bar: 20 µm. C) Quantitative analysis of area occupied by ZO-1. Data are reported as mean ± S.D. (*) $p<0.05$, (***) $p < 0.001$, (****) $p<0.0001$, two-way ANOVA. D) Quantitative analysis of nuclei area and number. Data are reported as mean ± S.D. (*) $p<0.05$, (**) $p<0.01$, (***) $p<0.001$, (****) $p<0.0001$, two-way ANOVA. N = 3, quantitative analyses were conducted on at least 5 different areas.

simplicity and inability to properly recapitulate human intestinal complexity.[23] Although CaCo-2 cells exhibit the brush border characteristic of the intestinal epithelium, they indeed lack crucial components of the in vivo environment, such as mucus production, which is essential for both pharmacokinetic and host-pathogen interaction studies.[24,25] An additional key parameter to model intestinal environment in vitro is the mucus thickness, as it changes during disease.[26] To address this, mucus-secreting cells such as HT29-MTX are employed either as an alternative to or in co-culture with CaCo-2 cells.[27] The proportion of goblet cells varies along the intestinal tract, ranging from 10% in the small intestine to 24% in the distal colon, and different studies suggested a variety of ratios for CaCo-2 and HT29-MTX cells.[28,29] Thus, more deep investigations are needed to

improve the in vitro intestinal models and to establish standardized procedures.

In recent years, novel culture systems, including cutting-edge organ-on-chip (OOC) technologies have been adopted to advance these cell culture models, by providing a 3D microenvironment and a dynamic medium flow, closely mimicking physiological conditions of the human gastrointestinal tract.[30,31] These innovations, which also include the application of shear stress, affecting cell behavior, are pivotal in improving the accuracy and relevance of in vitro studies, thereby bridging the gap between experimental models and in vivo clinical trials. In physiological conditions, cells are indeed constantly subjected to shear forces, which significantly influence cellular morphology, differentiation, and gene expression.[32–34] Moreover, incorporating a constant laminar fluid flow, these advanced in vitro models facilitate the testing compound diffusion and permeation across the tissue, advancing pharmacokinetic studies.

Among the most used gut-on-chip models, polydimethylsiloxane (PDMS)-based chips gained huge popularity, due to their cost-effectiveness and excellent optical imaging features. However, despite the numerous advantages,[35–37] it is important to remember that PDMS shows high protein binding properties, potentially leading to unreliable results in drug permeation studies.[38] Furthermore, multitude of these chips rely on gravity to induce media movement in the gut lumen and in the circulatory circuits, making the control of flow rate more challenging,[31] and finally failing in finely replicating in vivo intestinal flow conditions.

In this current study the innovative PDMS-free MIVO millifluidic device, previously adopted for pharmacokinetic (PK) and pharmacodynamic (PD) studies of different compounds for oncology,[39] skin application[40] and gut permeation,[41] was used to co-culture CaCo2:HT-29 cells. Final aim was the optimization of the dynamic flow culture conditions to develop a human intestinal in vitro model that provides physiological insights for translational research and pharmacological applications. To induce flow, a peristaltic pumping system with a finely tuneable flow rate was used to recapitulate both the blood-capillary and luminal flows at physiological velocities, in a unique double flow configuration. Intestinal cells maturation levels, mucus production, barrier function and permeability levels were characterized in comparison to a static control.

2. Results

2.1. Dynamic Culture Improves CaCo-2 Differentiation

Intestinal epithelial cells are constantly exposed to different mechanical forces, including fluid shear stress (FSS), in the gut lumen, on one side, and in the circulatory bloodstream feeding the tissue, on the other side. These forces are known to significantly alter cellular structure and function, enhancing tissue oxygen exchange, mucus production, microvilli development, tight junction expression, and cytoskeletal reorganization.[32,42] Recent studies have demonstrated stark morphological, functional, and phenotypical differences between intestinal cells cultured in static versus dynamic environments.[43,44] Despite this evidence, there is currently no detailed or systematic study on the effects of FSS under different flow rates on intestinal cell differentiation.

To this aim, a preliminary experiment was conducted on CaCo-2 monolayers to define the optimal flow rate, and associated velocities and FSS, allowing to achieve a reliable, complete and fast intestinal epithelium differentiation. The previously developed MIVO Single Flow millifluidic device was adopted for differentiation of CaCo-2 under dynamic conditions (**Figure 1A**). Flow rates of 0.4, 1, and 2 mL min^{-1} in the range of physiological velocities considering the millifluidic nature of the device were recapitulated in a closed circuit. A static control was also carried out in parallel.

Cell differentiation was verified by immunostaining against ZO-1 (Zonula Occludens 1, a protein expressed in tight junctions, TJ), after 7, 14, and 21 days. Interestingly, results highlighted important differences between static and dynamic culture condition. After 7 days, static-differentiated cells did not show any spatial organization of ZO-1 and TJ formation, while they started to organize an epithelium after 14 days, where ZO-1 was found expressed both intracellularly and in cell-cell junctions. A structurally organized and developed TJ network was observed only after 21 days of static differentiation (Figure 1B).

On the contrary, the presence of FSS in dynamic culture induced a significant increase in ZO-1 expression compared to static control, indicating enhanced tight junction formation and related cellular barrier integrity among cells. An initial and homogeneous spatial organization of TJ was visible already at earlier time point (7 days), especially under flow rates of 0.4 and 1 mL min^{-1}. In addition, at 14 and 21 days, a higher ZO-1 expression compared to static condition, with robust TJ assembly was observed in all the dynamic conditions. Intriguingly, dynamic culture under the flow rate of 1 mL min^{-1} exhibited a stronger ZO-1 expression after 14 and 21 days, compared to both 0.4 and 2 mL min^{-1}, inducing the formation of a more compacted gut epithelium.

Furthermore, the area occupied by ZO-1 was also quantified by using ImageJ (Figure 1C). Quantitative results confirmed the previous findings, showing that dynamic culture condition under 1 mL min^{-1} flow rate induced a stronger expression of ZO-1 compared to static condition ($p < 0.001$ at 14 and 21 days) and to both 0.4 ($p < 0.05$ at 14 days) and 2 mL min^{-1} ($p < 0.001$ at 14 days and $p < 0.05$ at 21 days) flow rates. Impressively, dynamic culture at flow rate of 1 mL min^{-1} achieved maturation levels in CaCo-2 cells comparable to those observed in 21-day static differentiation, within 7 days. Furthermore, ZO-1 expression continued to increase at 14 days and then maintained a high and constant plateau through to 21 days.

Quantitative analysis was also carried out on DAPI-nuclear staining picture, to compare number of nuclei between different culture conditions (Figure 1D). Dynamic culture at flow rate of 1 mL min^{-1} induced an increase in number of nuclei after 14 days, suggesting an induction of cell proliferation, that was not observed in the other culture setups.

Taken together, these data suggest that the flow rate of 1 mL min^{-1} was the optimal dynamic condition for inducing CaCo-2 differentiation, as it promoted an initial more effective cell proliferation, followed by a robust expression of ZO-1 and efficient organization of TJ. Furthermore, our findings also highlighted that dynamic culture conditions significantly reduce the time required to establish a fully differentiated gut barrier, with

a tight intestinal layer achieved after 1 week and complete differentiation occurring within a maximum of 14 days.

2.2. Different CaCo-2:HT-29 Ratios can Recapitulate both Physiological and Pathological Conditions

The luminal surface of gastrointestinal tract acts as a highly dynamic barrier consisting of a constantly renewing epithelial layer, covered by mucus.[45] Although mucus was traditionally viewed as a protector against mechanical damage and microbial invasion, recent research highlighted its symbiotic relationship with the commensal microbiome.[46–48] Furthermore, alterations in mucus structure and composition are also associated with serious diseases like inflammatory bowel disease.[49] This underscores the importance of a physiological mucus layer in in vitro models aimed at reliable disease modelling and host-microbiome interactions studying. Various in vitro cellular models have been developed, where epithelial CaCo-2 cells and goblet HT-29 cells are mixed in different ratios.[27,50,51] However, studies that thoroughly characterize the resulting mucus layer are limited, and a method standardization is mandatory to establish reliable and physiologically relevant in vitro screening tools.

Based on these considerations, a second step of optimization was performed with the aim of defining the best ratio for the co-culture of these two cell lines, to obtain an intestinal epithelium which more closely resembles the physiological situation. To this extent, three different ratios of CaCo-2:HT-29, in the physiological range (9:1, 6:1, and 3:1) were cultured and differentiated into the MIVO Single Flow chambers, for 14 days, by using the 1 mL min^{-1} flow rate selected in the first preliminary experiment. Differentiation of mono-cultures of CaCo-2 and HT-29 was also performed in parallel, in dynamic conditions, to deeper understand the contribution of each cell type for the model establishment (**Figure 2A**).

TEER measurement was conducted every 3–4 days as an indirect measure of intestinal barrier maturation (Figure 2B). Data showed that in 3:1 ratio TEER values rose from day 0 (51.58 ± 33.33 Ωcm^2) to day 7 (94.15 ± 9.78 Ωcm^2), reaching then a plateau and maintaining constant TEER values (Figure 2A), until the end of the culture (105.7 ± 19.94 Ωcm^2 at day 14). This was in accordance with data reported in literature showing that a 70/30 CaCo-2:HT-29 co-culture exhibit a maximum of TEER increase after 6 days of culture, maintaining then a plateau level, without any statistical difference.[51] In addition, 6:1 ratio exhibited a similar trend, with a TEER plateau after day 7 (127.4 ± 11.38 Ωcm^2), until the last day of maturation (127.1 ± 20.14 Ωcm^2), although it showed significantly higher TEER values at day 14, compared to 3:1 ratio ($p < 0.0001$). On the contrary, 9:1 ratio co-culture showed a less prominent plateau, with TEER values constantly rising from day 0 (69.94 ± 31.56 Ωcm^2) to day 7 (124.7 ± 29.36 Ωcm^2), and then slowing down but still maintaining a positive trend until the end of the culture (168.4 ± 39.12 Ωcm^2 at day 14). Notably, differences in epithelial resistance might be reconducted not only to a different epithelium maturation, but also to the cell types used to setup the model. TEER measurement is indeed very sensitive to the tightness of cell junctions and it has been widely described that HT-29 cell line generate a less tight epithelium compared to CaCo-2.[52] An internal control was indeed carried out, by differentiating mono-cultures of both CaCo-2 and HT-29. Interestingly, CaCo-2 exhibited significantly higher TEER values compared to the co-cultures and to HT-29 alone ($p < 0.0001$ to all), with a steady increase of TEER over time until day 7 (from 125.9 ± 2.49 Ωcm^2 at day 0 to 242.35 ± 37.2 Ωcm^2 at day 7). After day 7, similarly to 9:1 ratio, CaCo-2 showed a slowdown of TEER measurement, still maintaining a positive trend until the end of the culture (293.08 ± 16.05 Ωcm^2 at day 14). On the opposite, HT-29 did not present any change in TEER measurement during the culture, maintaining a constant epithelial resistance from day 0 to day 14 (Figure 2B).

Based on these considerations, the cell type used can strongly influence TEER measurements, which therefore cannot be relied upon as a solid and unequivocal indicator of gut epithelium maturation. Incorporating mucus-producing goblet cells into the model might indeed lead to a decreased transepithelial resistance, suggesting at first glance the establishment of an unstable and unreliable epithelium. However, this co-culture allows to develop a more physiological and relevant mucus-competent model.

As further analysis, immunostaining on tight junction protein ZO-1 was also performed, as an endpoint measurement of differentiation (Figure 2C). Despite the significant differences previously observed in electrical resistance, a high ZO-1 expression and comparable TJ organization was observed in all the culture conditions. This suggested the formation of a compacted gut epithelium in all conditions. The area occupied by ZO-1 was also quantified by using ImageJ and data are reported in Figure 2E, as percentage on total area. Quantitative results confirmed the previous findings, showing no statistical difference between the different cultures. Interestingly, these data suggest that while the expression of ZO-1 indicates the presence of tight junctions, it does not necessarily reflect their functionality or integrity. In fact, the functionality of the junctions, as measured by TEER, is likely to be greater with a higher number of CaCo-2 cells, as these cells are more effective at forming a tight and continuous barrier.

Furthermore, mucus production was also characterized by Alcian Blue staining. Results highlighted a mucus production which was in accordance with the different amounts of HT-29 cells in the three ratios considered (Figure 2D). Indeed, while a thick and dense mucus layer was found in HT-29 mono-cultures, consistently lower mucus was observed in the co-cultures. According to the percentage of seeded HT-29, higher mucus production was observed in 3:1 ratio compared to 9:1 ratio, where a very poor and thin mucus layer was detected. Interestingly, 6:1 ratio showed a mucus layer more similar to the co-culture with the highest concentration of HT-29, although it previously showed higher TEER values. Given these data, the 6:1 ratio was selected as the optimal balance for mucus production and barrier function, producing a thick, healthy mucus layer, while maintaining physiological TEER values and robust TJ organization. Indeed, under normal conditions, mucus coats the intestinal epithelium, forming a protective barrier that facilitates stool transit and shields the mucosa from pathogens and harmful substances.

Surprisingly, also CaCo-2 mono-cultures presented a partial and slight mucus production. Although differentiated CaCo-2 primarily have an absorptive phenotype, their ability to partially produce mucins has been indeed already described.[53,54]

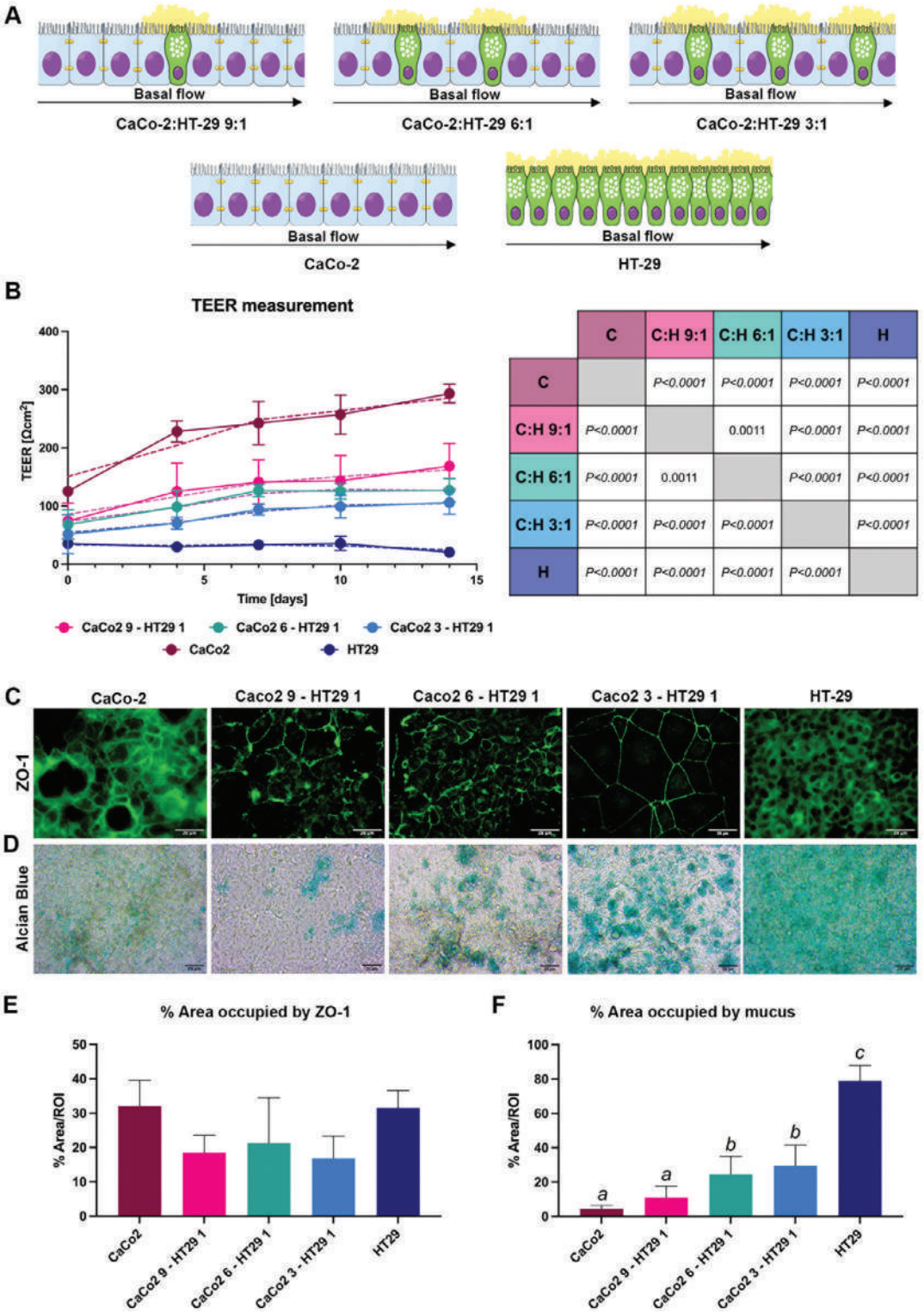

	C	C:H 9:1	C:H 6:1	C:H 3:1	H
C		P<0.0001	P<0.0001	P<0.0001	P<0.0001
C:H 9:1	P<0.0001		0.0011	P<0.0001	P<0.0001
C:H 6:1	P<0.0001	0.0011		P<0.0001	P<0.0001
C:H 3:1	P<0.0001	P<0.0001	P<0.0001		P<0.0001
H	P<0.0001	P<0.0001	P<0.0001	P<0.0001	

Figure 2. Optimization of CaCo-2:HT-29 best ratio after differentiation in dynamic conditions. A) Schematic representation of the experimental design. Different ratios of CaCo-2 and HT-29 were differentiated for 14 days in dynamic conditions, in MIVO Single Flow. B) TEER measurement of CaCo-2:HT-29 co-cultured cells, at different ratios and different time points. Data are reported as mean ± S.D. Double entry table shows the p values of multiple comparison, two-way ANOVA. C) Representative figures of ZO-1 immunostaining after 14 days of differentiation in MIVO Single Flow. Scale bar: 20 µm. D) Representative figures of Alcian Blue staining after 14 days of differentiation in MIVO Single Flow. Scale bar: 20 µm. Quantitative analysis of area occupied by ZO-1 E) and by mucus F). Data are reported as mean ± S.D. Values with shared letters are not significantly different ($P > 0.05$) according with one-way ANOVA. N = 9, quantitative analyses were conducted on at least 5 different areas.

However, the amount of mucus produced by CaCo-2 monocultures was significantly lower compared to co-cultures and to HT-29 (more than 6X).

The area occupied by mucus was also quantified by using ImageJ and data are reported in Figure 2F, as percentage on total area. Quantitative results confirmed the previous findings, showing a different presence of mucus in the different models.

Taken together, these data suggest that the presented model might be used as a physiologically relevant gut model, suitable as in vitro platform for predictive pharmacokinetic and host-pathogen interaction studies. Additionally, our results also demonstrated that a fine tuning of different cell types might help in reproducing different physiological and pathological conditions.

2.3. Dynamic Flow in Apical Side Triggered the Initial Formation of Villi-Like Structures

As previously mentioned, gastrointestinal lumen is an extremely fluid-dynamic environment, where the need to protect the body from external treats has to coexist with the necessity to permit nutrient absorption.[55]

After demonstrating the beneficial effect of a dynamic FSS in the basal side of cell culture, resembling the capillary bloodstream, a second fluidic flow was included in the apical compartment, to recapitulate the gut luminal environment. For this purpose, the selected CaCo-2:HT-29 6:1 ratio was cultured in MIVO Double Flow chambers (Dynamic DF), allowing to replicate both capillary and luminal circulations (flow rate of 0.2 mL min^{-1} and 0.07 mL min^{-1} respectively) through basal and apical dynamic closed circuits, respectively. A proper static control and the Single Flow dynamic condition (Dynamic SF) were also included (**Figure 3A**).

TEER measurement was conducted every 3–4 days as an indirect measure of intestinal barrier maturation (Figure 3B). Interestingly, TEER plateau was reached after 5–7 days in all the conditions, confirming previous findings. Moreover, Dynamic DF differentiation enable to reach significantly higher TEER values at the end of the culture, compared to both Dynamic SF ($p < 0.05$) and Static condition ($p < 0.0001$), suggesting the development of a more mature gut epithelium.

Proper formation of intestinal barrier after 10 days of differentiation in static, MIVO Single Flow and MIVO Double Flow was also monitored using Fluorescein IsoThioCyanate (FITC)-dextran 20 KDa (FD20, Sigma Aldrich, St. Louis, MO) tissue permeability assay (Figure 3C). Notably, FD20 permeability showed results mirroring a similar trend compared to TEER measurements. Intestinal cell layers differentiated in Dynamic DF displayed indeed significantly lower permeability to FD20 in comparison to both the Dynamic SF and the Static conditions ($p < 0.001$ and $p < 0.0001$, respectively). Moreover, showing a permeability rate of 1.17 ± 0.13% apical FD20*cm^{-1} h^{-1}, Dynamic DF-intestinal epithelium was impressively consistent with in vivo permeability data. In recent studies, healthy animals exhibited a serum concentration of FD at 0.8% of the orally administered FD dose (red dotted line in Figure 3C).[56]

Since FSS has a known ability to trigger microvilli development,[57] differentiated intestinal layers were further investigated by SEM analysis (Figure 3D), which showed a clear rugosity on cell surface, representing the typical intestinal brush border formed by microvilli (yellow arrows in Figure 3D), in all the conditions. Interestingly, both Dynamic SF and Dynamic DF conditions presented more prominent 3D structures (yellow circles in Figure 3D) compared to static control, suggesting an initial triggering of villi-like formations. To confirm this hypothesis, intestinal cell layers were histologically analysed. Haematoxylin/Eosin (HE, Figure 3E) and Alcian Blue/PAS staining (Figure 3F) were performed to characterize cell morphology and mucus layer, respectively. Static control revealed a poorly organized layer of cells, where epithelial and goblet cells are mixed together without any tissue structure. Alcian Blue staining indicated the presence of positive cells, actively secreting mucus, scattered throughout the entire cell layer (blue arrows in Figure 3F). Furthermore, no mucus layer on the surface could be noticed at the analysed stage. On the other hand, Dynamic SF showed a greater organization of the cell layer, where the cell nuclei appear aligned in rows, indicating an initial polarization of the epithelium. Additionally, Alcian Blue staining revealed an evident mucus layer on the apical surface of the cell layer (blue arrows in Figure 3F), which was not observed in the static control. Interestingly, in line with previous results, Dynamic DF exhibits a more pronounced organization and alignment of cell nuclei and a curvature of the intestinal layer, suggesting the initial formation of villi structures, as hypothesized by SEM analysis. Furthermore, Dynamic DF intestinal layer exhibited a more clear and prominent formation of microvilli on the apical side of the cells (red arrows in Figure 4D), forming the typical brush border. Contrary to Dynamic SF, Dynamic DF did not display a thick mucus layer, although regions of Alcian blue positivity were detectable. This phenomenon may be attributed to the influence of apical dynamic flow, which likely facilitates the removal of excess mucus and properly affect the intestinal cells behavior as in vivo. While mucus is crucial for gut homeostasis, it poses indeed challenges for drug delivery since drugs must permeate it to reach the epithelium and be absorbed.[58] The mucus is a complex hydrogel with multiple barrier levels and a constant turnover. This network is dynamic, creating a limited time window for drug permeation.[59] Static models often fail to mimic the physiological environment, as they do not adequately capture the dynamic characteristics of the barrier in vivo. Therefore, it is essential to develop models that incorporate these dynamic processes to better predict how drugs will behave within the mucus layer under actual physiological conditions.

Tight junction formation is a critical aspect of the maturation of the intestinal cell layer since proper maturation of the cell layer includes the development and establishment of tight junctions, that were characterized by immunostaining against the tight junction protein ZO-1 (**Figure 4A**).

Interestingly, only the intestinal cells differentiated under dynamic conditions, both Dynamic SF and Dynamic DF, were able to develop a high ZO-1 expression and an organized tight junction structure. On the other side, although static control expressed ZO-1 at the cellular level, it was not able to develop the typical hexagonal shape characteristic of mature intestinal barrier with tight cellular junctions.

In addition, villin expression was also investigated (Figure 4B). Villin is the primary actin-bundling protein that accumulates at

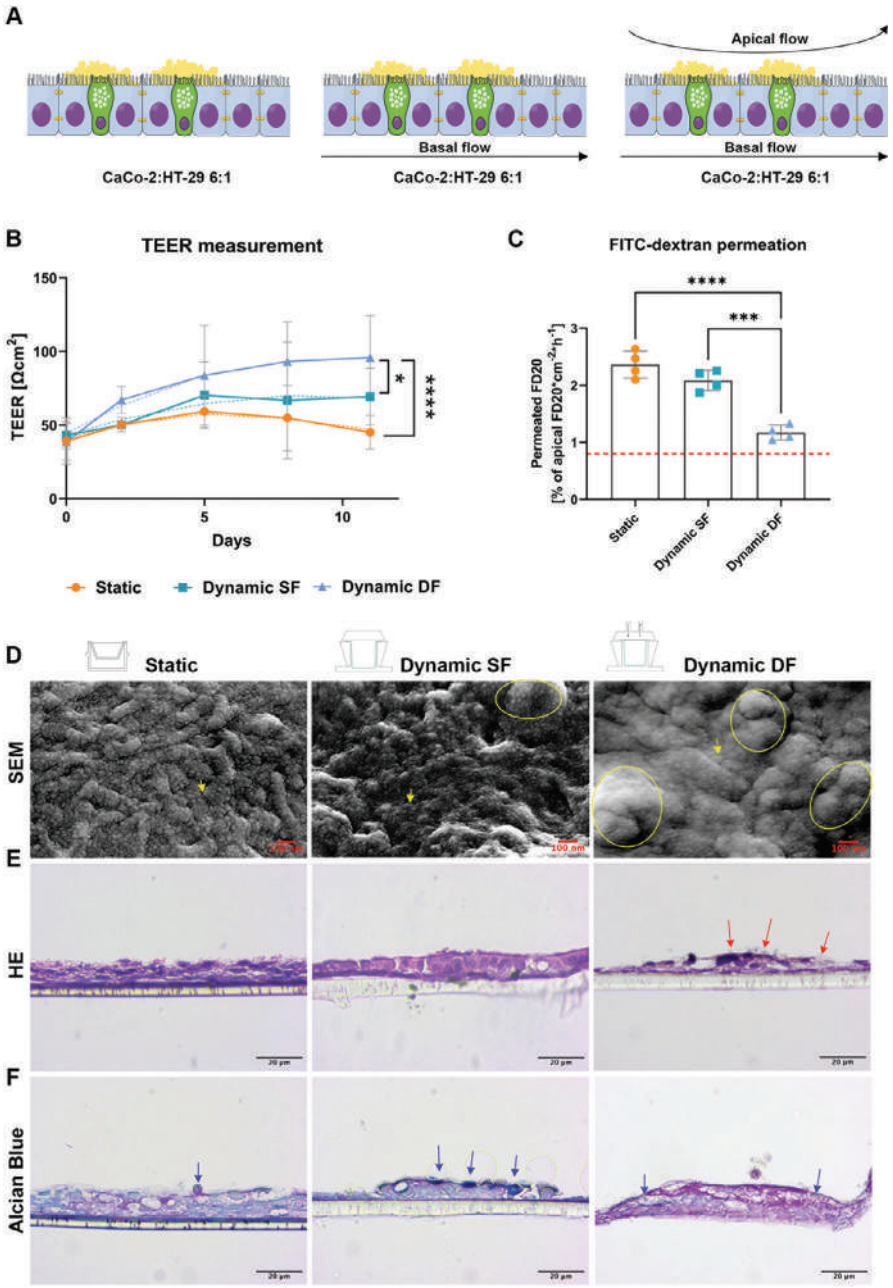

Figure 3. Comparison of CaCo-2:HT-29 differentiation in static, Dynamic SF and Dynamic DF conditions. A) Schematic representation of CaCo-2:HT-29 6:1 co-culture in Static condition, in MIVO Single Flow (Dynamic SF), and in MIVO Double Flow (Dynamic DF). B) TEER measurement of CaCo-2:HT-29 co-cultured cells, at different ratio and different time points. Data are reported as mean ± S.D. (*) $p < 0.05$, (****) $p < 0.0001$, two-way ANOVA. N = 6 C) FITC-dextran permeability in CaCo-2:HT-29 intestinal epithelia, expressed in percentage of apical FD20*$cm^{-2}h^{-1}$. Red dotted line displays the reference data of in vivo studies. Data are reported as mean ± S.D. (***) $p < 0.001$, (****) $p < 0.0001$, one-way ANOVA. N = 4 D) SEM micrographs of CaCo-2:HT-29 differentiated in static, Dynamic SF and Dynamic DF condition. Scale bar: 100 nm. Yellow arrows and yellow circles point out microvilli and 3D structures, respectively. Representative figures of HE E) and Alcian Blue F) staining after 10 days of differentiation in static conditions, Dynamic SF and Dynamic DF. Scale bar: 20 µm. Red arrows point out microvilli, blue arrows indicate mucus. N = 4.

the apical surface of enterocytes,[60] playing a crucial role in initiating, organizing, and forming the rigid structure of the microvilli core.[61,62] Undifferentiated intestinal epithelial cells exhibit low levels of villin and do not form brush borders.[63] As villin expression increases, it correlates with cell differentiation and villi and microvilli assembly.[64] Furthermore, overexpression of villin in fibroblasts and other non-epithelial cells leads to the formation of surface microvilli and reorganization of the microfilament network.[65] Therefore, villin levels are key in regulating actin reorganization and microvillus density.

Interestingly, Static condition did not show any villin expression, confirming that the intestinal layer was still in an

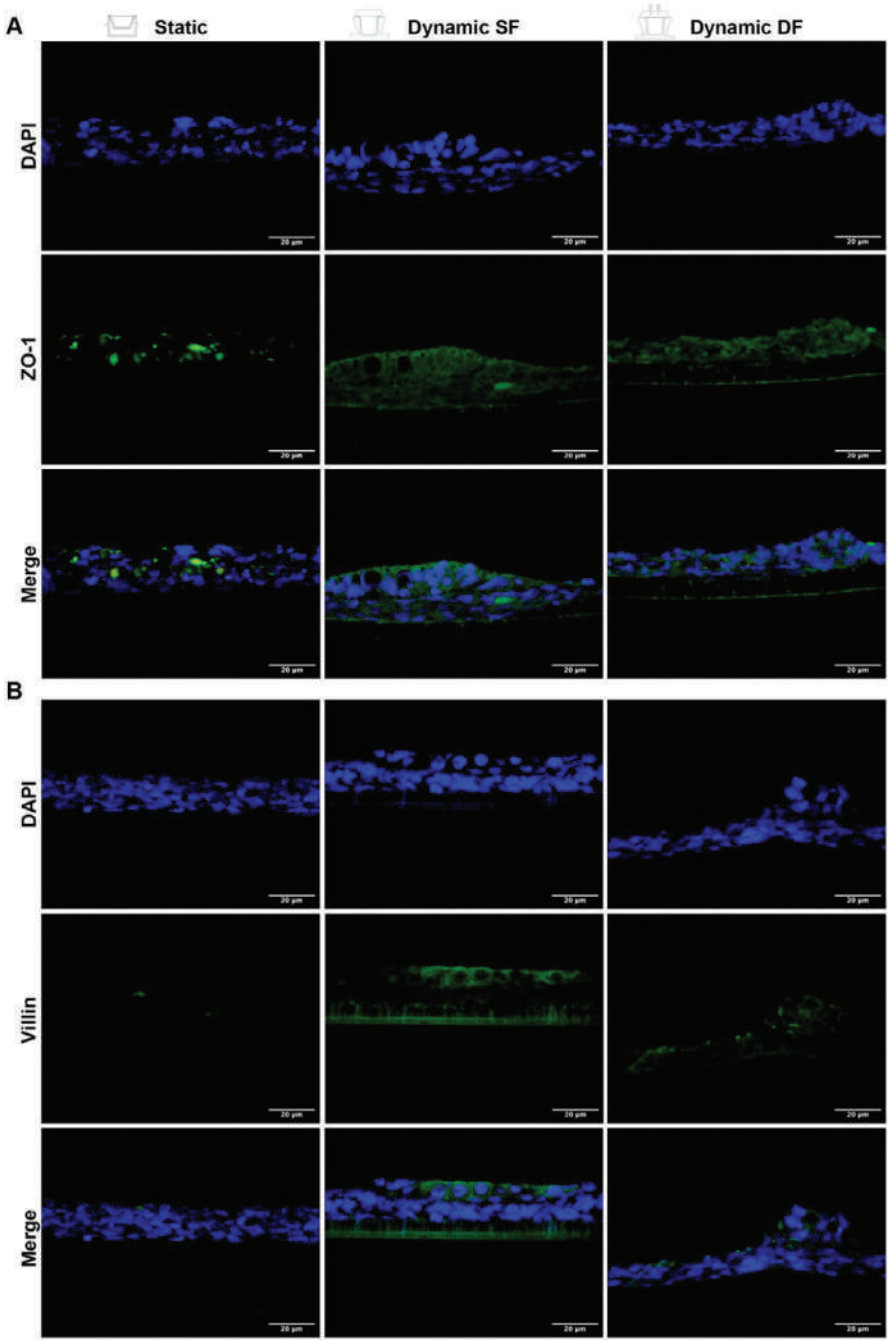

Figure 4. Immunostaining against ZO-1 of CaCo-2:HT-29 differentiated in static, Dynamic SF and Dynamic DF conditions. Representative figures of ZO-1 A) and Villin B) immunostaining after 10 days of differentiation. Top panels show DAPI staining, highlighting cell nuclei, middle panels show ZO-1 or Villin and bottom panels report the merge of channels. Scale bar: 20 µm.

undifferentiated stage after 10 days in culture. In contrast, the dynamic SF condition showed villin expression in the most apical cell layer, where the nuclei appeared aligned, confirming the more differentiated stage of these cells and the initial cytoskeletal organization of the intestinal layer. Lastly, the dynamic DF condition exhibited villin expression only in the apical surface, although it was not continuous and partially fragmented, particularly localized in areas of swelling, suggesting the initial formation of a villous structure.

Taken together, these results demonstrated that the combination of tuned CaCo-2:HT-29 co-cultures with Double Flow, resembling both gut luminal and capillary flows allows for the generation of a reliable and more physiological intestinal layer, more similar to the in vivo small intestine compared to in vitro currently available static models, being also suitable for

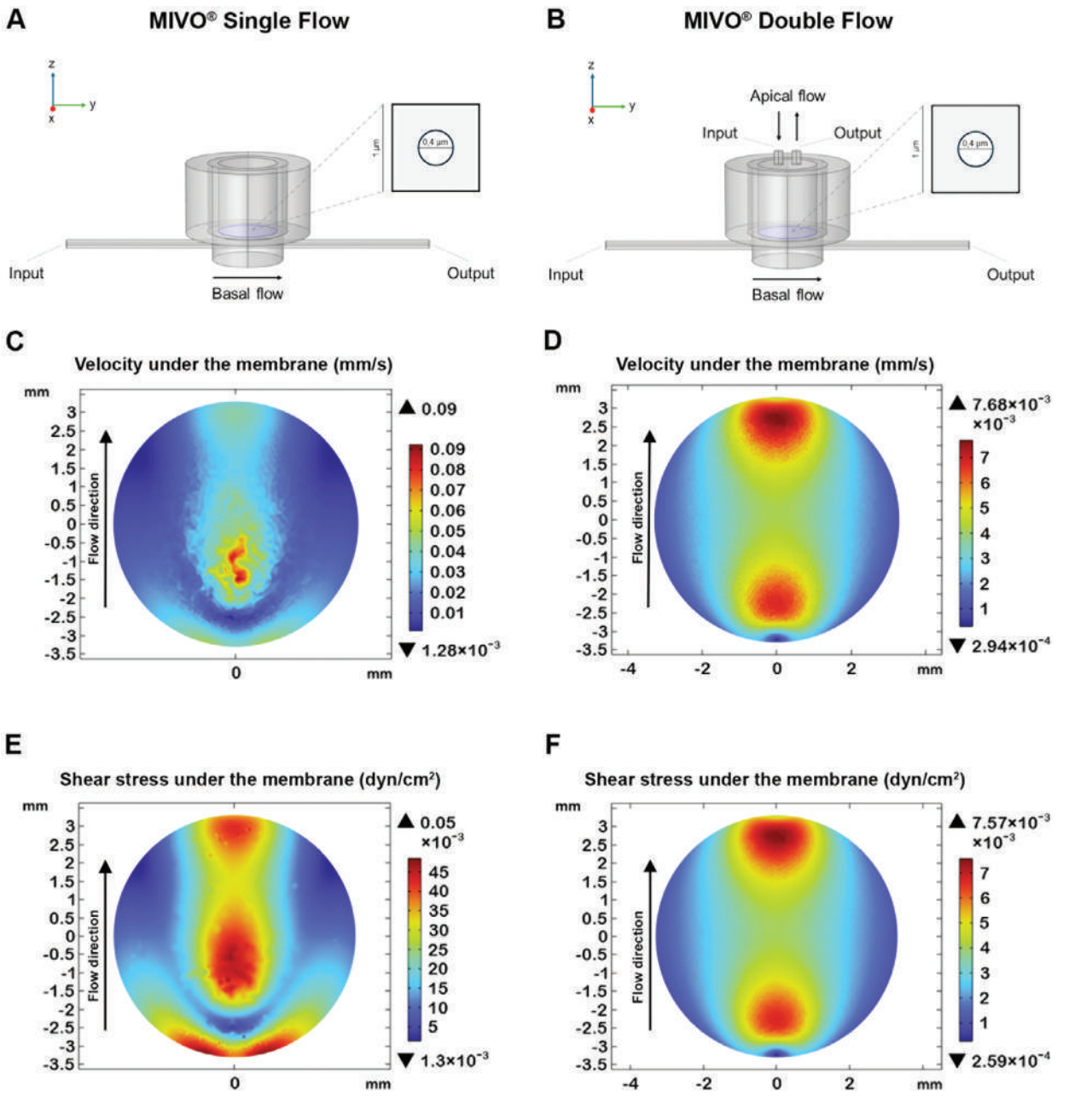

Figure 5. Computational Fluid Dynamic Simulation of MIVO Single Flow and Double Flow. Planar geometry of MIVO Single Flow A) and MIVO Double Flow B). Arrows show the flow direction. Velocity profiles under the intestinal cell layer (mm s^{-1}) in MIVO Single Flow C) and MIVO Double Flow D). Shear stress under the intestinal cell layer (dyn cm^{-2}) in MIVO Single Flow E) and MIVO Double Flow F).

pharmacokinetic studies and predictive absorption studies of orally administered drugs.

2.4. Computational Fluid Dynamic Simulation

A computational analysis of the fluid dynamics within the MIVO Single Flow and MIVO Double Flow platform was also performed, and the fluid shear stress (FSS) and velocity profiles on the cells surface were evaluated (**Figure 5**). Median, mean and mode values, extrapolated through MATLAB, are shown in **Table 1**.

In MIVO Single Flow configuration, higher shear stress values were found close to the inlet source and in the central part under the membrane where cells were seeded, while lower shear stress areas were observed laterally and far from the inlet source. In MIVO Double Flow configuration, higher FSS were found along the direction of the flow. Overall, in both configurations, FSS values remain within the gastrointestinal layer physiological range (0.002–0.08 dyn cm^{-2}).[45]

Table 1. Shear stress (SS) and velocity statistical indexes on the cellularized membrane surface in MIVO Single Flow and MIVO Double Flow.

	Shear Stress [dyn cm^{-2}]		Velocity [mm s^{-1}]	
	MIVO Single Flow	MIVO Double Flow	MIVO Single Flow	MIVO Double Flow
Mean	0.0205	0.0025	0.0206	0.0026
Median	0.0178	0.0019	0.018	0.002
Mode	0.0013	2.59×10^{-4}	0.0013	0.0011
Physiological values	0.002–0.08 [45]			

Similar distribution was observed in terms of velocities for the two configurations.

2.5. Barrier Function Model and TEER Measurements

Trans-endothelial/epithelial electrical resistance (TEER) is a non-invasive and quantitative technique to monitor cell barrier properties. TEER measurements assess the electrical resistance of biological barrier models, including endothelial and epithelial monolayers, both in in vitro and in vivo conditions. The main application of this type of measurements is to predict the biological membrane integrity during cultivation and in response to different chemical conditions, such as drug testing.[66]

TEER values were assessed on intestinal cell layers by measuring voltage induced by an applied current, and a corresponding electrical model of the cell barrier was established, where the current can flow using two paths across the cellular barrier, transcellular and paracellular route. When the current passes across the barrier through the transcellular path, it encounters two different impedances: the cell membrane resistance ($R_{membrane}$) and the membrane capacitance ($C_{membrane}$), placed in parallel. On the contrary, going across the cell monolayer through the paracellular path between the cells, the current will engage a resistance due to cell tight junctions (R_{TJ}). For completeness, the electrical model also considers the resistance of the cell culture medium (R_{medium}) and the capacitor of the TEER electrodes ($C_{electrodes}$) (**Figure 6A**).

Since TEER measurements are tipically conducted at low frequencies (i.e., 12.5 Hz), the electrical parallel between $R_{membrane}$ and $C_{membrane}$ in the transcellular route can be simplified, considering only $R_{membrane.}$ Moreover, being $R_{membrane} >> R_{TJ}$, the resulting electrical parallel between $R_{membrane}$ and R_{TJ} can be further simplified as R_{TJ} alone. Indeed, as also reported in literature, the paracellular path is the main factor influencing TEER measurements of cellular layer.[67]

In addition, the device used to measure TEER operates with an alternating current at a sufficiently high frequency to nullify the contribution of the capacitor $C_{electrodes,}$ which can be therefore disregarded. Similarly, R_{medium} can be ignored in the electrical model, since its value is measured during the experimental procedure (i.e., blank measurement) and then subtracted from the total measured value.

Based on these considerations, R_{TJ} is the unique remaining parameter of the cell barrier model.

When different cells are co-cultured (e.g., CaCo-2 and HT-29), multiple R_{TJ} resistances, corresponding to each cell type, are connected in parallel. Furthermore, since HT-29 actively secrete mucus, its presence over the cellular layer need to be included in the electrical model, as a further resistance R_{mucus}, placed in series (Figure 6B,C). In the specific case of co-cultures of CaCo-2:HT-29 cells, the hereby proposed electrical model takes into account also the different ratio between CaCo-2 and HT-29 and the resulting mucus deposition.

The electrical model proposed in this study aimed at expanding the commonly used model to better explain and predict the influence of varying amounts of CaCo-2 and HT-29 cells on TEER values. In this co-culture, the cell monolayer is characterized by the two cell types, described by the two resistances R_{CaCo} and R_{HT29}, connected in parallel. In particular, each cellular resistance (R_{CaCo} and R_{HT29}) represents the electrical parallel of all the cells of the corresponding type. These resistances depend on the cell number of each cell type, and consequently on their occupied area (i.e., A_{CaCo2} and A_{HT29}) (Equations 1 and 2), which is correlated to the insert size and the percentage of one cell population to the other one (i.e., % HT29). The mucus resistance is modelled by both resistivity parameters ρ_{mucus} and the area covered by mucus itself (A_{mucus}) (Equation 3).

$$R_{CaCo_2=} TEER_{CaCo_2}/A_{CaCo_2} \quad (1)$$

$$R_{HT29=} TEER_{HT29}/A_{HT29} \quad (2)$$

$$R_{mucus=} A_{mucus} * \rho_{mucus} \quad (3)$$

In this scenario, the first Cells Co-Culture TEER (C^3-TEER) model, characterized by the three different and constant parameters ρ_{mucus}, $TEER_{CaCo}$ and $TEER_{HT29}$ were here developed.

By fitting experimental data under different CaCo-2:HT-29 ratios, it was possible (i) to successfully validate the C^3-TEER model (resulting Mean Squared Error MSE = 60.47$(\Omega cm^2)^2$ and R^2 = 0.9934), and (ii) to calculate the three model parameters. The fitted model is reported in Figure 6D.

Interestingly, resistance due to the mucus layer showed to have a very little impact on the total resistance, especially at lower concentrations of HT-29. For this reason, the C^3-TEER model can be considered successfully reliable even with fewer degrees of freedom (DOF), ignoring the mucus resistance. Based on this, data fitting was carried out by using only the ratio of CaCo-2 and HT-29 (i.e., independent variable) and the corresponding measured TEER values (i.e., dependent variable), after 14 days of incubation. The new model, shown in Figure 6E, is still very accurate (resulting Mean Squared Error = 65.03 $(\Omega cm^2)^2$ and R^2 = 0.9929), especially at low percentage of HT-29, although having less parameters.

These results show that the proposed C^3-TEER model is extremely predictive of the electrical characteristics of a cell barrier

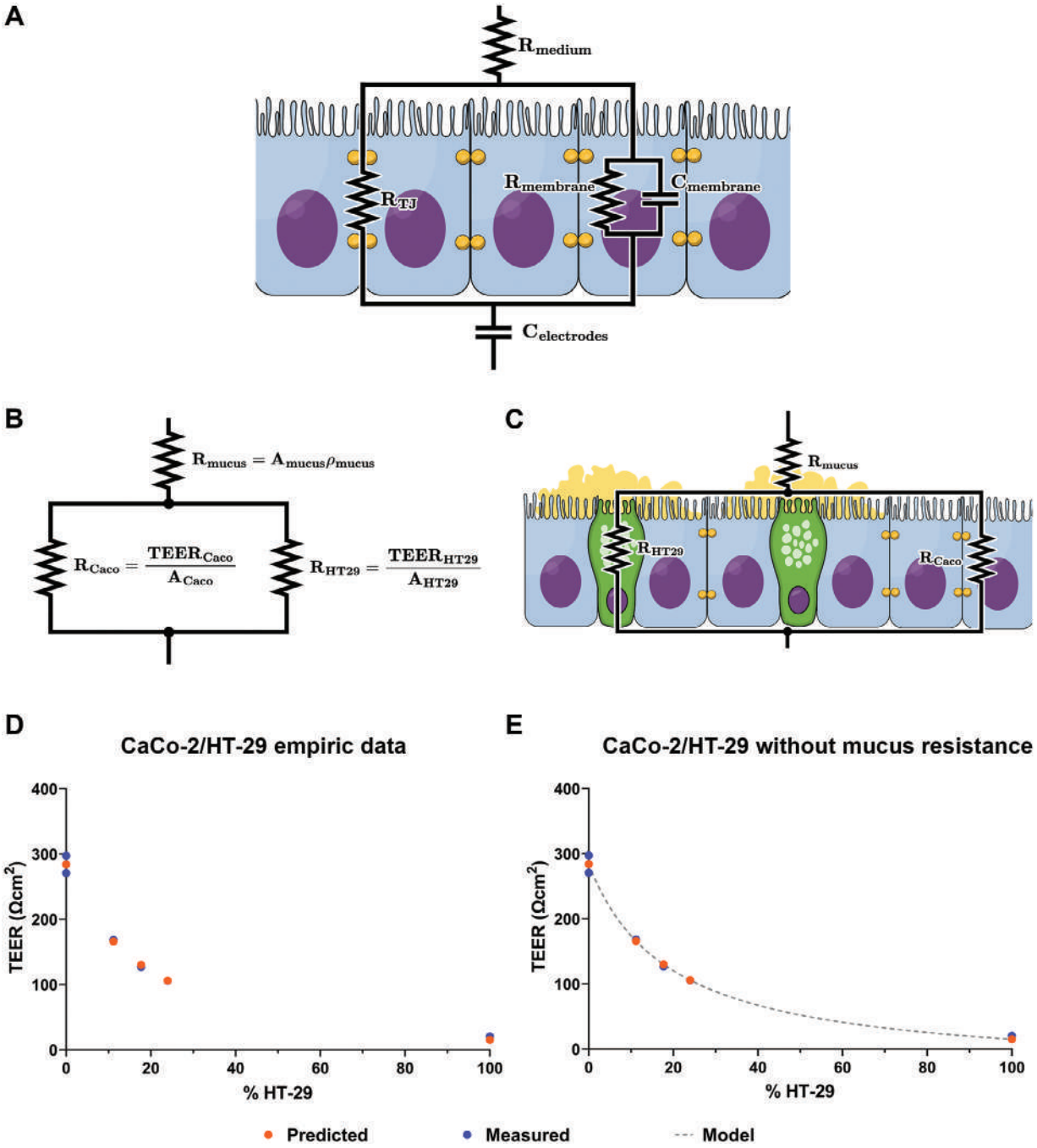

Figure 6. Equivalent electrical circuit describing a cell monolayer. A) R_{medium} is the resistance of the culture medium, $C_{electrodes}$ is the capacitive effect of the measuring electrodes, R_{TJ} is the resistance of the tight junctions between the cells, $R_{membrane}$ and $C_{membrane}$ are the resistance and capacitance of the cell membranes. B) A_{mucus}, A_{CaCo} and A_{HT29} are the areas occupied by mucus, CaCo-2 and HT-29 respectively, expressed in cm^2; ρ_{mucus} is the resistivity of mucus, expressed in $\Omega\ cm^{-2}$, while $TEER_{CaCo}$ and $TEER_{HT29}$ represent the resistance of the cell barrier normalized to the area, same as a regular TEER value, and are expressed in Ωcm^2. C) Simplified electrical model of a monolayer composed of CaCo-2 and HT-29 cells and a mucus layer is shown. D) Model of CaCo-2:HT-29 cell barrier fitted with empirical data. E) Model of CaCo-2:HT-29 cell barrier without mucus resistance.

developed with a CaCo-2:HT-29 co-culture. More interestingly, the C^3-TEER model enables to correctly predict the expected measures of TEER values of an intestinal cell model based on a known ratio of Caco-2 to HT-29 cells, and thus give useful insights about the timing and readiness of cells maturation.

3. Discussion

The human gut has recently attracted significant scientific interest due to its critical roles in nutrient digestion and drug absorption, as well as its influence on the functioning of other

organs and the development of various diseases. Despite its integral role in maintaining homeostasis, there remains a significant knowledge gap on gut mechanisms and host-microbe interactions, largely due to the limitations of traditional models.[68]

Historically, animal models and 2D in vitro static culture have been the primary tools for studying human physiology and responses to pathogens, diseases, and drugs.[69,70] However, these models often fall short of accurately representing human-specific conditions.

To address this gap, gut-on-chip technology has emerged as a novel tool. These models utilize microfluidic technology and cell biology to simulate the structure, function, and microenvironment of the human gut, including villi structures, intestinal peristalsis, oxygen gradients, and even components of the immune system.[71–73]

Despite advancements in technology, most of these gut-on-chip systems are based on over-miniaturized platforms, lacking the ability to simultaneously coculture different intestinal cells and finely control a double flow configuration mimicking the apical gut lumen and circulatory flow circuit experienced by the tissue. This work introduces, for the first time, the optimization of a new gut-on-chip built on a millifluidic platform, allowing for the culture of clinically relevant-sized intestinal tissues and a double and independent flow condition. Furthermore, the presented study demonstrates that flow rate optimization is a crucial parameter for faithfully reproducing the velocity and shear stress that intestinal cells experience in vivo both in the gut lumen and in the bloodstream feeding the tissue.

Our results demonstrated that dynamic culture conditions allowed for the differentiation of an intestinal layer in a third of the time compared to traditional static in vitro systems, ensuring better outcomes that more closely simulate in vivo situation, in a shorter timeframe. These findings are consistent with previous reports showing that the application of a physiological FSS can induce significant phenotypical and functional changes in CaCo-2[32,74] and HT-29[75] monolayers, as well as in jejunal human enteroids,[76] enhancing cell maturation and promoting an in vivo-like cell reorganization. As widely documented in the literature, FSS can indeed influence tissue structure and function by enhancing the transport of oxygen and nutrients, which improve intestinal cells differentiation, also triggering microvilli and villi formation.[32,57] This accelerated cell differentiation under dynamic conditions supports the use of the proposed model as a valuable tool for drug development, as it allows for more physiologically relevant testing in a reduced timeframe, which translates to significant time and cost savings.

Another key parameter when modelling intestinal tissue is the mucus layer. Intestinal mucus acts as a barrier between the external environment and the epithelium, selectively permits nutrient and drug intake, regulates the symbiosis with the intestinal microbiota, and protects the epithelium from pathogen attacks.[77] To investigate these intricate relationships, it is essential to create models that can faithfully replicate the in vivo environment, including mucus thickness, as it changes based on pathological states. However, the amount of mucus present in the intestine in vivo varies depending on the species, diet, and potential pathological conditions. For instance, in patients with Crohn's disease, the mucus layer in the descending colon thickens, whereas it thins in individuals with ulcerative colitis compared to healthy patients.[26] Accurately replicating these changes in in vitro models is paramount for understanding disease mechanisms and developing effective treatments.

This study illustrates how manipulating the ratio between different cell types allows for the reproduction of physiological conditions emulating diverse healthy or pathological states. By varying the concentration of mucus-secreting goblet cells, the proposed model might simulate conditions characterized by either thicker or thinner mucus layers, depending on the specific inflammatory context and application scenario. The results presented in this study provide valuable insights into the formation of a functional intestinal epithelium under dynamic culture conditions, highlighting the influence of cell ratio and the complex interplay between CaCo-2 and HT-29 cells in creating a more physiologically relevant model. Specifically, our findings show that co-cultures with varying ratios of CaCo-2 and HT-29 cells can strongly impact the TEER measurements, which decreased parallelly with the increase of HT-29 percentage. These results are consistent with previous literature, which has explored the effects of cell type and ratio on intestinal barrier function.[51,52] However, our study extends these observations by incorporating dynamic culture conditions that more accurately simulate in vivo conditions.

Moreover, the C^3-TEER electrical models here described and successfully validated enables to cross-correlate the TEER values of the epithelial layer with the CaCo-2:HT-29 cells ratio, finally providing for the first time a predictive model of the proper and functional barrier function values to be obtained for a certain ratio of cells. In addition, starting from an intact intestinal tissue whose TEER is measured, the C^3-TEER model enables to infer about the cellular composition and related mucus production.

Our results also highlighted the importance of the establishment of a second apical flow, to recapitulate the lumen environment: indeed, this dynamic double flow has played a crucial role in triggering the formation of 3D gut structures. Furthermore, double flow configuration also allowed for the creation of an intestinal layer with permeability characteristics very similar to the in vivo small intestine and physiological conditions,[56] being therefore suitable for predictive pharmacokinetic and absorption studies of orally administered drugs. While the current study represents a significant advancement in mimicking the intestinal barrier in vitro, there are still some areas that could be further explored. Although permeability data serve as an in vitro-in vivo cross-validation and useful first approximation of the model translational potential, direct measurements of other key physiological parameters, such as colonic enzyme activities, released metabolites, and substrate degradation, would provide a more comprehensive understanding of the system's physiological relevance and its alignment with human intestinal functions. These measurements are crucial for assessing the true physiological relevance of the model, particularly in comparison to the human colon.[78]

The proposed model also paves the way for the investigation of host-microbiota and host-pathogen interactions, where a static model would be inadequate, due to the risk of bacteria overgrowth on the host tissue, with subsequent impairment of cell viability.[79] On the contrary, the introduction of a dynamic flow guarantees the persistence of attached microbiota and

its metabolites, while enhancing the clearance of organic acids and removing the unbound bacterial cells, thus preventing their overgrowth.[79,80] A dynamic flow in the apical compartment is therefore essential to ensure proper interaction between bacteria and the intestinal mucosa and their adhesion to the mucus layer.

Additionally, the proposed experimental model might be easily applied also in pharmaceutical research for predictive studies of bioaccessibility and bioavailability of poorly soluble drugs. A traditional static model with CaCo-2 cells seeded on permeable porous membrane would indeed be inefficient, since the drug is not removed from the solution as it would occur in vivo. This artifact drives higher supersaturation levels which leads to drug precipitation on the cell monolayer, compromising reliability of results and potentially causing cell damage.[81]

Further studies will be addressed to induce proper cellular polarization. Whilst our model induces the initiation of 3D formation, representing an advancement over the current gold standard, it does not produce a fully formed intestinal layer. Additionally, the model could be improved by introducing a bacterial component to simulate the intestinal microbiota.

4. Conclusions

In conclusion, this study highlights the potential of a millifluidic gut-on-chip model that mimics the dynamic conditions of the human gut. The optimization of flow rates and co-culture ratios enables a more accurate representation of intestinal differentiation, barrier function, and mucus production. The incorporation of the C^3-TEER model further provides predictive insights into barrier integrity based on cell composition.

While the model shows promise for drug absorption studies, disease modeling, and host-microbe interactions, future improvements, such as the inclusion of enzyme assays and microbiota components, will further enhance its physiological relevance.

This platform finally paves the way for more efficient and physiologically accurate in vitro models for intestinal research.

5. Experimental Section

Cell Culture: CaCo-2 cells (ATCC-HTB-37, ATCC, Manassas, Virginia, USA) were cultured in RPMI medium (EuroClone, Milan, Italy) supplemented with 20% FBS (EuroClone), 1% Penicillin/Streptomycin mixture (EuroClone) and 2 mM L-Glutammine (EuroClone).

HT-29 cells (ATCC HTB-38) were cultured in RPMI medium supplemented with 10% FBS, 1% Penicillin/Streptomycin mixture and 2 mM L-Glutammine. Both cell lines were subcultured at 80% confluence and seeded for expansion at the density of 1×10^5 cells cm^{-2}.

For intestinal cell layer differentiation, both CaCo-2 and HT-29 cells were trypsinized, mixed in different ratios (Caco-2:HT-29 1:0, 9:1, 6:1, 3:1, and 0:1) and seeded onto permeable porous inserts (Greyner Bio-One, Kremsmünster, Austria). Cells were then cultured in RPMI medium, supplemented with 10% FBS, 1% Penicillin/Streptomycin mixture and 2 mM L-Glutammine (complete medium), in static condition, in a 24-well plate for 48 h, to allow proper cell attachment. After 48 h, cells were either moved in MIVO device (React4life, Genoa, Italy) for differentiation in dynamic conditions or kept in static as control.

Cells were cultured in a humified incubator at 37 °C for a maximum of 21 days and medium was changed twice per week.

Dynamic Culture: MIVO Organ on Chip: The MIVO device was used as diffusive culture chamber able to host human tissues under physiological conditions, providing a fluidic circulation below the tissues mimicking the human circulatory system. The receiver compartment was connected to a peristaltic pump inducing a monodirectional flow at capillary velocities.

A first preliminary experiment was conducted on CaCo-2 monolayers to define the optimal flow rate to induce intestinal epithelium differentiation. CaCo-2 were seeded on 24-well inserts as described above and, after 48 h of static culture, they were moved into the MIVO Single Flow chambers, one insert for each sterile chamber, for differentiation under dynamic conditions. The R100-1J peristaltic pump (React4life) was used to recapitulate the flow rates of 0.4, 1, and 2 mL min^{-1}, corresponding to physiological flow range, in a closed circuit. A static control was also carried out. Differentiation was conducted for 21 days, after which the cells were fixed for further analyses.

A second experiment was aimed at determining the CaCo-2:HT-29 optimal ratio. Five different ratios of Caco-2:HT-29 (1:0, 9:1, 6:1, 3:1 and 0:1) were seeded on 24-well inserts as described above and, after 48 h of static culture, they were moved into the MIVO Single Flow chambers, one insert for each sterile chamber, for differentiation under dynamic conditions. The flow rate of 1 mL min^{-1} was recapitulated by using peristaltic pump, in a closed circuit. Differentiation was conducted for 14 days, after which the cells were fixed for further analyses.

Finally, the optimal Caco-2:HT-29 6:1 ratio was seeded on 24-well inserts as described above and, after 48 h of static culture, cells were moved into either MIVO Single Flow or MIVO Double Flow chambers, one insert for each sterile chamber, for differentiation under dynamic conditions. The MIVO Double Flow system allows to replicate both capillary and luminal circulations through basal and apical dynamic closed circuits, respectively. The peristaltic pump was adopted to recapitulate a flow rate of 0.21 mL min^{-1} in the basal circuit, and a flow rate of 0.07 mL min^{-1}, in the apical circuit. A proper static control was also included. Differentiation was conducted for 10 days, after which the cells were used for further analyses.

Measurement of Barrier Integrity and Electrical Modeling of the Cell Barrier: Impedence of the intestinal cell layers was measured by using a Millicell ERS-2 (Merck, Darmstadt, Germany), as indirect measurement of intestinal layers development. It is based on the Ohm's law method. In this simple method, a current I is used to stimulate the cell barrier, while simultaneously measuring the voltage V across it and computing the corresponding resistance R according to Ohm's law (Equation 4).

$$R = \frac{V}{I} \tag{4}$$

Resistance measurements were performed every 2–3 days, right after medium change, by immersing the electrode with the shorter tip in the insert and the longer tip in the MIVO chamber. The resistance of a blank control was also measured, by adding medium to an insert without cells (R_{blank}). The final resistance is then calculated according to the Equation 5.[66]

$$R_{final} = R - R_{blank} \tag{5}$$

The resulting resistance value R_{final} is then normalized by multiplying with the cells seeding area, to obtain electrical TEER values independent from the area itself.[67] TEER values are reported as Ω*cm^2, where TEER of cell layer is the final resistance multiplied by the cellular area (i.e., surface area of the insert S_I) (Equation 6).

$$TEER\ (\Omega * cm^2) = R_{final}\ (\Omega) * S_I\ (cm^2) \tag{6}$$

FITC-Dextran Trans-Epithelial Permeability Assay: Proper formation of intestinal barrier after 10 days of differentiation in static, MIVO Single Flow and MIVO Double Flow was monitored using Fluorescein IsoThioCyanate (FITC)-dextran 20 KDa (FD20, Sigma Aldrich, St. Louis, MO) tissue permeability assay. After the differentiation period, cells were washed twice with PBS, and DMEM w/o phenol red (EuroClone) containing 1 mg mL^{-1} FD20 was then added to the apical compartment (250 µL). DMEM w/o phenol red (500 µL) was added in the basal compartment and cells were incubated at 37 °C, 5% CO^2 and 98% relative humidity for 1.5 h.

After incubation time, medium from basal compartment was collected to quantify the amount of FD20 permeated through the barrier. The quantity of FITC-dextran accumulated into the receiver chamber was quantified based on the emitted fluorescence of permeated FD20 in the basal compartment. Fluorescence was read on an Infinite M nano (Tecan, Männedorf, Switzerland) using 490/520 nm excitation/emission rate. A calibration curve was done to correlate the fluorescence intensity and the amount (μg mL^{-1}) of FD20 present in the solution and to calculate the quantity of permeated FD20.

Scanning Electron Microscopy: Scanning Electron Microscopy (SEM) analysis was conducted on intestinal cell layers after 10 days of differentiation in static, MIVO Single Flow and MIVO Double Flow. Samples were gently de-hydrated by using progressively increasing concentrations of ethanol. Following, the permeable porous membrane was removed from the insert, and samples were placed on an adhesive active carbon patch fixed to an aluminium disc. To avoid charging, the sample was coated with a thin layer of gold, which does not alter the morphology of the tissue. An electron beam energy of 20 keV, which enhances the morphological contrast obtained with secondary electrons, and an aperture of 30 μm, which generates a narrow beam current for optimum resolution at high magnification, were used for imaging with a positive biased Everhart-Thornley detector.

Histology and Immunostaining: After cells maturation, samples were fixed in 3.7% formaldehyde (Merck, Darmstadt, Germany) for 10 min at room temperature. Following fixation, the samples were washed 3 times and stored in PBS.

To visualize the mucus produced by HT-29 cells, Alcian blue (AB) staining was performed on 2D-cultured intestinal cell layers. Acidic mucins were stained with 0.1% Alcian Blue for 20 min. Images were acquired by using a Nikon Eclipse Ts2-FL. The area occupied by Mucins, their average area and total number per ROI (= Region of Interest) were quantified by using Fiji ImageJ.

For immunostaining, 2D-cultured intestinal cell layers were permeabilized with 0.1% Triton in PBS for 10 min, washed in PBS and incubated with 2% BSA in PBS for 1 h at RT to inhibit the unspecific binding. Cells were incubated with primary antibody overnight at 4 °C (anti ZO1, ab96587, 1:200, Abcam, rabbit polyclonal Ab in 0.2% BSA in PBS).

After primary incubation, cells were washed three times in PBS and incubated with secondary antibody at RT for 1 h (goat-anti-rabbit AlexaFluor 488-conjugated antibody, A-11070, Thermofisher Scientific in 0.2% BSA in PBS). Cells were then washed three times in PBS and stained for nuclear content with DAPI, for 15 min at RT. Following three washes in PBS, images were acquired by using a Nikon Eclipse Ts2-FL.

For paraffin embedding and histological procedures, cell-hosting membranes were first cut out from their plastic holder with a scalpel, removed with tweezers and transferred in a properly labelled histological cassette. Samples were then dehydrated in ethanol, and paraffin-embedded. Cross sections of 5 μm were cut (by using microtome RM2165, Leica Microsystems, Wetzlar, Germany), dewaxed and stained according to the appropriate histological analysis: haematoxylin and eosin staining to observe cell organization and alcian blue/PAS staining to detect mucopolysaccharides.

For immunostaining, paraffin-cleared sections were boiled in an epitope retrieval solution (citrate buffer pH 6.0), and then let cool down to RT for 20 min. Boiled sections were permeabilized with 0.1% Triton in PBS for 20 min, washed in PBS and incubated with 2% BSA in PBS for 1 h at RT. Slides were incubated primary antibodies (ZO1 or Villin, 1:200, ab97512 Abcam) overnight at 4 °C and then with AlexaFluor 488-conjugated secondary antibody at RT for 2 h. After DAPI staining, performed for 15 min at RT, slides were layered with Dako Fluorescent Mounting medium, covered with coverslips, and photographed with a Nikon Eclipse Ts2-FL, for image acquisition. Images were then processed with Fiji-Image J. All fluorescence images were acquired with the same settings and magnification.

CFD Simulation: A computational analysis of the fluid dynamics within the MIVO devices was carried out to predict the fluid velocity and shear stress perceived by a monolayer of intestinal cells cultured on a commercial 24-well insert. For the model geometry, the design of the MIVO device, was simplified to consider only the essential parts and the insert, and sketched as follows. Both the Single-Flow and the Double-Flow configurations were considered.

The study was performed employing the Free and Porous Media Flow module of Comsol Multiphysics 6.0, considering 1) a laminar flow regime, 2) an incompressible Newtonian fluid, 3) the 24-well insert membrane as a porous medium. Navier-Stokes Equation (Equation 7) for the conservation of momentum and the continuity law for conservation of mass Equation (Equation 8) were used:

$$\rho\left(\frac{\partial \boldsymbol{u}}{\partial t}+\boldsymbol{u}\cdot\nabla\boldsymbol{u}\right)=-\nabla p+\mu\nabla^2\boldsymbol{u} \tag{7}$$

$$\rho\ (\nabla\cdot\boldsymbol{u})=0 \tag{8}$$

where u is the velocity and p the pressure across the circuit. The culture medium density ρ and dynamic viscosity μ values were for water at room temperature. As initial conditions, the velocity field and the pressure were considered null. For the Single-flow configuration, it was imposed a flow rate of 1 mL min^{-1} to induce fluid motion, according to the experimental set up, while a zero-pressure was set as output, avoiding the backflow. Additionally, a no-slip boundary condition was applied. Furthermore, the Darcy's law (Equation 9) was considered for the 24-well insert membrane:

$$\boldsymbol{u}=-\frac{\kappa}{\mu}\nabla p \tag{9}$$

where κ (m^2) is the permeability of the membrane, which depends on the porosity ϵ_p and on the diameter of the pores d, according to Sheiddeger.[82] (Equation 10)

$$\kappa=\varepsilon_p\,\frac{d^2}{32} \tag{10}$$

The porosity of 13% was determined by considering the pores diameter (0.4 μm) and pore density (10^8 cm^{-2}). Differently, in the Double-flow configuration, input flow rates of 0.21 mL min^{-1} and 0.07 mL min^{-1} were considered for the basal and apical flows, respectively. The boundary conditions were identical to the single-flow setup. An iterative geometric multigrid (GMRES) algorithm was employed to solve the equations for the steady-state condition. MATLAB was used to process the data.

Statistical Analysis: Data were analyzed with GraphPad Prism 9.3 software. Two-way ANOVA was used for TEER measurement comparison over time and for ZO-1 analysis in CaCo-2 under different flow rates. One-way ANOVA was used for FITC-dextran, ZO-1 and mucus quantification in different co-culture conditions. Level of significance was set at $p < 0.05$ ($*p < 0.05$, $**p < 0.01$, $***p < 0.001$, $****p < 0.0001$). Number of replicates for each experiment are reported in figure legends. Data are shown as mean ± SD.

Acknowledgements

This project has received funding from the European Union's Horizon Research and Innovation programme under the Marie Skłodowska-Curie (HORIZON-MSCA-2021-DN-01) grant agreement No. 101 072 717. The authors warmly thank Prof. Rodolfo Quarto for his kind support in the histological analyses.

Conflict of Interest

M.A., S.S., M.E.F.P., G.B., and J.F. are employed by the company React4life S.p.A. The remaining authors declare that the research was conducted in the absence of any commercial or financial relationships that could be construed as a potential conflict of interest.

Author Contributions

M.E.F.P. and M.A. contributed equally to this work.

Data Availability Statement

The data that support the findings of this study are available from the corresponding author upon reasonable request.

Keywords

barrier function, C^3-TEER model, dynamic culture, gut-on-chip, in vitro human intestine model, millifluidic, organ-on-chip

Received: October 3, 2024
Revised: January 13, 2025
Published online:

[1] E. Salvo-Romero, C. Alonso-Cotoner, C. Pardo-Camacho, M. Casado-Bedmar, M. Vicario, *Revista espanola de enfermedades digestivas* **2015**, *107*, 686.
[2] M. Camilleri, K. Madsen, R. Spiller, B. G. Van Meerveld, G. N. Verne, *Neurogastroenterol. Motil.* **2012**, *24*, 503.
[3] M. Lindner, A. Laporte, S. Block, L. Elomaa, M. Weinhart, *Cells* **2021**, *10*, 2062.
[4] P. A. Billat, E. Roger, S. Faure, F. Lagarce, *Drug Discov Today* **2017**, *22*, 761.
[5] T. Murakami, *Expert Opin Drug Discov* **2017**, *12*, 1219.
[6] C. Chelakkot, J. Ghim, S. H. Ryu, *Exp. Mol. Med.* **2018**, *50*, 1.
[7] M. Vancamelbeke, S. Vermeire, *Expert Rev. Gastroenterol. Hepatol.* **2017**, *11*, 821.
[8] J. R. Turner, *Nat. Rev. Immunol.* **2009**, *9*, 799.
[9] L. W. Peterson, D. Artis, *Nat. Rev. Immunol.* **2014**, *14*, 141.
[10] N. Shi, N. Li, X. Duan, H. Niu, *Mil Med Res* **2017**, *4*, 14.
[11] A. M. Mowat, W. W. Agace, *Nat. Rev. Immunol.* **2014**, *14*, 667.
[12] N. Di Tommaso, A. Gasbarrini, F. R. Ponziani, *Int J Environ Res Public Health* **2021**, *18*, 12836.
[13] S. Alqahtani, L. A. Mohamed, A. Kaddoumi, *Expert Opin Drug Metab Toxicol* **2013**, *9*, 1241.
[14] B. Belà, M. M. Coman, M. C. Verdenelli, A. Gramenzi, G. Pignataro, D. Fiorini, S. Silvi, *Veterinary Sciences* **2024**, *11*, 19.
[15] K. Papadimitriou, G. Zoumpopoulou, B. Foligné, V. Alexandraki, M. Kazou, B. Pot, E. Tsakalidou, *Front Microbiol* **2015**, *6*, 58.
[16] J. L. Round, S. K. Mazmanian, *Nat. Rev. Immunol.* **2009**, *9*, 313.
[17] P. J. Turnbaugh, R. E. Ley, M. A. Mahowald, V. Magrini, E. R. Mardis, J. I. Gordon, *Nature* **2006**, *444*, 1027.
[18] J. S. Loh, W. Q. Mak, L. K. S. Tan, C. X. Ng, H. H. Chan, S. H. Yeow, J. B. Foo, Y. S. Ong, C. W. How, K. Y. Khaw, *Signal Transduction Targeted Ther.* **2024**, *9*, 37.
[19] B. De Pessemier, L. Grine, M. Debaere, A. Maes, B. Paetzold, C. Callewaert, *Microorganisms* **2021**, *9*, 353.
[20] A. Y. K. Thye, Y. R. Bah, J. W. F. Law, L. T. H. Tan, Y. W. He, S. H. Wong, S. Thurairajasingam, K. G. Chan, L. H. Lee, V. Letchumanan, *Biomedicines* **2022**, *10*, 1037.
[21] E. W. Esch, A. Bahinski, D. Huh, *Nat Rev Drug Discov* **2015**, *14*, 248.
[22] M. Hu, J. Ling, H. Lin, J. Chen, *Optimization in Drug Discovery*, Springer, Berlin **2004**, 19.
[23] A. Fedi, C. Vitale, G. Ponschin, S. Ayehunie, M. Fato, S. Scaglione, *J. Controlled Release* **2021**, *335*, 247.
[24] M. Calvigioni, A. Panattoni, F. Biagini, L. Donati, D. Mazzantini, M. Massimino, C. Daddi, F. Celandroni, G. Vozzi, E. Ghelardi, *Microbiol Spectr* **2023**, *11*, 336.
[25] M. Herath, S. Hosie, J. C. Bornstein, A. E. Franks, E. L. Hill-Yardin, *Front Cell Infect Microbiol* **2020**, *10*, 520859.
[26] R. D. Pullan, G. A. O. Thomas, M. Rhodes, R. G. Newcombe, G. T. Williams, A. Allen, J. Rhodes, *Gut* **1994**, *35*, 353.
[27] P. Hoffmann, M. Burmester, M. Langeheine, R. Brehm, M. T. Empl, B. Seeger, G. Breves, *PLoS One* **2021**, *16*, 0257824.
[28] I. Lozoya-Agullo, F. Araújo, I. González-Álvarez, M. Merino-Sanjuán, M. González-Álvarez, M. Bermejo, B. Sarmento, *Mol Pharm* **2017**, *14*, 1264.
[29] N. Panse, P. M. Gerk, *Int. J. Pharm.* **2022**, *624*, 122004.
[30] S. Taavitsainen, K. Juuti-Uusitalo, K. Kurppa, K. Lindfors, P. Kallio, M. Kellomäki, *Frontiers in Lab on a Chip Technologies* **2024**, *2*, 1337945.
[31] D. P. Thomas, J. Zhang, N. T. Nguyen, H. T. Ta, *Biosensors* **2023**, *13*, 136.
[32] L. C. Delon, Z. Guo, A. Oszmiana, C. C. Chien, R. Gibson, C. Prestidge, B. Thierry, *Biomaterials* **2019**, *225*, 119521.
[33] S. Scaglione, D. Wendt, S. Miggino, A. Papadimitropoulos, M. Fato, R. Quarto, I. Martin, *J Biomed Mater Res A* **2008**, *86*, 411.
[34] A. Marrella, A. Fedi, G. Varani, I. Vaccari, M. Fato, G. Firpo, P. Guida, N. Aceto, S. Scaglione, *PLoS One* **2021**, *16*, e0245536.
[35] A. Ayoib, N. A. A. A. Karim, U. Hashim, *International Journal of Nanoelectronics and Materials (IJNeaM)* **2024**, *17*, 143.
[36] S. P. Kojic, G. M. Stojanovic, V. Radonic, *Sensors* **2019**, *19*, 1719.
[37] M. Annabestani, P. Esmaeili-Dokht, M. Fardmanesh, *Sci. Rep.* **2020**, *10*, 16513.
[38] M. W. Toepke, D. J. Beebe, *Lab Chip* **2006**, *6*, 1484.
[39] A. Fedi, C. Vitale, M. Fato, S. Scaglione, *Bioengineering (Basel)* **2023**, *10*, 10020270.
[40] I. Pulsoni, M. Lubda, M. Aiello, A. Fedi, M. Marzagalli, J. von Hagen, S. Scaglione, *SLAS Technol* **2022**, *27*, 161.
[41] A. Marrella, P. Buratti, J. Markus, G. Firpo, M. Pesenti, T. Landry, S. Ayehunie, S. Scaglione, H. Kandarova, M. Aiello, *ALTEX – Alternatives to animal experimentation* **2020**, *37*, 255.
[42] Y. Juste-Lanas, S. Hervas-Raluy, J. M. García-Aznar, A. González-Loyola, *APL Bioeng.* **2023**, *7*, 31501.
[43] M. Lindner, A. Laporte, S. Block, L. Elomaa, M. Weinhart, *Cells* **2021**, *10*, 10082062.
[44] C. Beaurivage, A. Kanapeckaite, C. Loomans, K. S. Erdmann, J. Stallen, R. A. J. Janssen, *Sci. Rep.* **2020**, *10*, 21475.
[45] M. Lindner, A. Laporte, S. Block, L. Elomaa, M. Weinhart, *Cells* **2021**, *10*, 10082062.
[46] J. F. Sicard, G. Le Bihan, P. Vogeleer, M. Jacques, J. Harel, *Front Cell Infect Microbiol* **2017**, *7*, 278172.
[47] J. Fang, H. Wang, Y. Zhou, H. Zhang, H. Zhou, X. Zhang, *Exp. Mol. Med.* **2021**, *53*, 772.
[48] A. S. Luis, G. C. Hansson, *Cell Host Microbe* **2023**, *31*, 1087.
[49] C. Schultsz, F. M. Van den Berg, F. W. T. Kate, G. N. J. Tytgat, J. Dankert, *Gastroenterology* **1999**, *117*, 1089.
[50] O. Reale, A. Huguet, V. Fessard, *Chemosphere* **2021**, *273*, 128497.
[51] A. Ferraretto, M. Bottani, P. De Luca, L. Cornaghi, F. Arnaboldi, M. Maggioni, A. Fiorilli, E. Donetti, *Biosci. Rep.* **2018**, *38*, 20171497.
[52] C. R. Kleiveland, C. R. Kleiveland, *The Impact of Food Bioactives on Health: In Vitro and Ex Vivo Models*, Springer, Berlin **2015**, p. 135.
[53] A. Akbari, A. Lavasanifar, J. Wu, *Acta Biomater.* **2017**, *64*, 249.
[54] R. H. Dosh, N. Jordan-Mahy, C. Sammon, C. L. Le Maitre, *Sci. Rep.* **2019**, *9*, 1812.
[55] R. Eri, M. Chieppa, *Front Immunol* **2013**, *4*, 00323.
[56] W. Panpetch, P. Phuengmaung, P. Hiengrach, J. Issara-Amphorn, T. Cheibchalard, N. Somboonna, S. Tumwasorn, A. Leelahavanichkul, *Int. J. Mol. Sci.* **2022**, *23*, 7050.

[57] S. Miura, K. Sato, M. Kato-Negishi, T. Teshima, S. Takeuchi, *Nat. Commun.* **2015**, *6*, 8871.
[58] B. H. Bajka, N. M. Rigby, K. L. Cross, A. Macierzanka, A. R. Mackie, *Colloids Surf B Biointerfaces* **2015**, *135*, 73.
[59] M. E. V. Johansson, *PLoS One* **2012**, *7*, 0041009.
[60] S. P. George, Y. Wang, S. Mathew, K. Srinivasan, S. Khurana, *J. Biol. Chem.* **2007**, *282*, 26528.
[61] M. B. Heintzelman, M. S. Mooseker, *Curr. Top. Dev. Biol.* **1992**, *26*, 93.
[62] K. R. Fath, D. R. Burgess, *Curr. Biol.* **1995**, *5*, 591.
[63] C. Huet, C. Sahuquillo-Merino, E. Coudrier, D. Louvard, *J. Cell Biol.* **1987**, *105*, 345.
[64] B. Dudouet, S. Robine, C. Huet, C. Sahuquillo-Merino, L. Blair, E. Coudrier, D. Louvard, *J. Cell Biol.* **1987**, *105*, 359.
[65] E. Frlederich, C. Huet, M. Arpin, D. Louvard, *Cell* **1989**, *59*, 461.
[66] H. Nazari, J. Shrestha, V. Y. Naei, S. R. Bazaz, M. Sabbagh, J. P. Thiery, M. E. Warkiani, *Biosens. Bioelectron.* **2023**, *234*, 115355.
[67] K. Benson, S. Cramer, H. J. Galla, *Fluids Barriers CNS* **2013**, *10*, 1.
[68] Y. Xiang, H. Wen, Y. Yu, M. Li, X. Fu, S. Huang, *J Tissue Eng* **2020**, *11*, 2041731420965318.
[69] R. T. Borchardt, *AAPS J.* **2011**, *13*, 323.
[70] F. Hugenholtz, W. M. de Vos, *Cell. Mol. Life Sci.* **2018**, *75*, 149.
[71] M. Calatayud, O. Dezutter, E. Hernandez-Sanabria, S. Hidalgo-Martinez, F. J. R. Meysman, T. Van De Wiele, *FASEB J.* **2019**, *33*, 3985.
[72] D. Huh, G. A. Hamilton, D. E. Ingber, *Trends Cell Biol.* **2011**, *21*, 745.
[73] G. S. Park, M. H. Park, W. Shin, C. Zhao, S. Sheikh, S. J. Oh, H. J. Kim, *Stem Cell Rev. Rep.* **2017**, *13*, 321.
[74] C. A. M. Fois, A. Schindeler, P. Valtchev, F. Dehghani, *Biomed. Microdevices* **2021**, *23*, 55.
[75] M. Lindner, A. Laporte, S. Block, L. Elomaa, M. Weinhart, *Cells* **2021**, *10*, 2062.
[76] J. Yin, L. Sunuwar, M. Kasendra, H. Yu, C. M. Tse, C. C. Talbot, T. Boronina, R. Cole, K. Karalis, M. Donowitz, *Am J Physiol Gastrointest Liver Physiol* **2020**, *320*, G258.
[77] L. Sardelli, D. P. Pacheco, A. Ziccarelli, M. Tunesi, O. Caspani, A. Fusari, F. Briatico Vangosa, C. Giordano, P. Petrini, R. S. C. Adv, **2019**, *9*, 15887.
[78] L. L. Von Moltke, D. J. Greenblatt, J. Schmider, C. E. Wright, J. S. Harmatz, R. I. Shader, *Biochem. Pharmacol.* **1998**, *55*, 113.
[79] A. Beterams, K. De Paepe, L. Maes, I. J. Wise, H. De Keersmaecker, A. Rajkovic, D. Laukens, T. Van de Wiele, M. C. Arroyo, *FASEB J.* **2021**, *35*, e21992.
[80] H. J. Kim, D. Huh, G. Hamilton, D. E. Ingber, *Lab Chip* **2012**, *12*, 2165.
[81] J. Keemink, C. A. S. Bergström, *Pharm. Res.* **2018**, *35*, 74.
[82] A. E. Scheidegger, *The Physics of Flow Through Porous Media*, Edition 3rd, University of Toronto Press, **1974**, http://www.jstor.org/stable/10.3138/j.ctvfrxmtw.

